

Revealing Color Forces with Transverse Polarized Electron Scattering

W. Armstrong,^{1,2} H. Kang,³ A. Liyanage,⁴ J. Maxwell,^{5,6} J. Mulholland,⁵ L. Ndukum,⁷ A. Ahmidouch,⁸ I. Albayrak,⁴ A. Asaturyan,⁹ O. Ates,⁴ H. Baghdasaryan,⁵ W. Boeglin,¹⁰ P. Bosted,⁶ E. Brash,^{11,6} C. Butuceanu,¹² M. Bychkov,⁵ P. Carter,¹¹ C. Chen,⁴ J.-P. Chen,⁶ S. Choi,³ M.E. Christy,⁴ S. Covrig,⁶ D. Crabb,⁵ S. Danagoulian,⁸ A. Daniel,¹³ A.M. Davidenko,¹⁴ B. Davis,⁸ D. Day,⁵ W. Deconinck,¹⁵ A. Deur,⁶ J. Dunne,⁷ D. Dutta,⁷ L. El Fassi,^{16,7} C. Ellis,⁶ R. Ent,⁶ D. Flay,¹ E. Frlez,⁵ D. Gaskell,⁶ O. Geagla,⁵ J. German,⁸ R. Gilman,¹⁶ T. Gogami,¹⁷ J. Gomez,⁶ Y.M. Goncharenko,¹⁴ O. Hashimoto,^{17,*} D. Higinbotham,⁶ T. Horn,⁶ G.M. Huber,¹² M. Jones,⁸ M.K. Jones,⁶ N. Kalantarians,^{5,18} H-K. Kang,³ D. Kawama,¹⁷ C. Keith,⁶ C. Keppel,^{4,6} M. Khandaker,¹⁹ Y. Kim,³ P.M. King,¹³ M. Kohl,⁴ K. Kovacs,⁵ V. Kubarovsky,^{6,20} Y. Li,⁴ N. Liyanage,⁵ W. Luo,²¹ D. Mack,⁶ V. Mamyas,⁵ P. Markowitz,¹⁰ T. Maruta,¹⁷ D. Meekins,⁶ Y.M. Melnik,¹⁴ Z.-E. Meziani,¹ A. Mkrtchyan,⁹ H. Mkrtchyan,⁹ V.V. Mochalov,¹⁴ P. Monaghan,⁴ A. Narayan,⁷ S.N. Nakamura,¹⁷ A. Nuruzzaman,⁷ L. Pentchev,¹⁵ D. Pocanic,⁵ M. Posik,¹ A. Puckett,²² X. Qiu,⁴ J. Reinhold,¹⁰ S. Riordan,⁵ J. Roche,¹³ O.A. Rondón,⁵ B. Sawatzky,¹ M. Shabestari,^{5,7} K. Slifer,²³ G. Smith,⁶ L.F. Soloviev,¹⁴ P. Solvignon,^{2,*} V. Tadevosyan,⁹ L. Tang,⁴ A.N. Vasiliev,¹⁴ M. Veilleux,¹¹ T. Walton,⁴ F. Wesselmann,²⁴ S. Wood,⁶ H. Yao,¹ Z. Ye,⁴ J. Zhang,⁵ and L. Zhu⁴

(SANE Collaboration)

¹Temple University, Philadelphia, PA

²Argonne National Laboratory, Argonne, IL

³Seoul National University, Seoul, Korea

⁴Hampton University, Hampton, VA

⁵University of Virginia, Charlottesville, VA

⁶Thomas Jefferson National Accelerator Facility, Newport News, VA

⁷Mississippi State University, Starkville, MS

⁸North Carolina A&M State University, Greensboro, NC

⁹Yerevan Physics Institute, Yerevan, Armenia

¹⁰Florida International University, Miami, FL

¹¹Christopher Newport University, Newport News, VA

¹²University of Regina, Regina, SK, Canada

¹³Ohio University, Athens, OH

¹⁴Kurchatov Institute - IHEP, Protvino, Moscow region, Russia

¹⁵William & Mary, Williamsburg, VA

¹⁶Rutgers University, New Brunswick, NJ

¹⁷Tohoku University, Tohoku, Japan

¹⁸Virginia Union University, Richmond, VA

¹⁹Norfolk State University, Norfolk, VA

²⁰Rensselaer Polytechnic Institute, Troy, NY

²¹Lanzhou University, Lanzhou, Gansu, People's Republic of China

²²University of Connecticut, Storrs, CT

²³University of New Hampshire, Durham, NH

²⁴Xavier University, New Orleans, LA

(Dated: September 19, 2022)

The Spin Asymmetries of the Nucleon Experiment (SANE) measured two double spin asymmetries (nearly transverse and longitudinal) using a polarized proton target and polarized electron beam at two beam energies, 4.7 GeV and 5.9 GeV. A large-acceptance open-configuration detector package identified scattered electrons at 40° and covered a wide range in Bjorken x ($0.3 < x < 0.8$). Proportional to an average color Lorentz force, the twist-3 matrix element, \tilde{d}_2^p , was extracted from the measured asymmetries at Q^2 values ranging from 2.0 to 6.0 GeV². The data display the opposite sign compared to most quark models including the lattice result and an unexpected scale dependence. Furthermore when combined with the neutron data in the same Q^2 range the results suggest a flavor independent average color Lorentz force.

Today, it is accepted that Quantum Chromodynamics (QCD), the gauge theory of strong interactions, plays a central role in our understanding of nucleon structure at the heart of most visible matter in the universe. QCD successfully describes many observables in high energy scattering processes where the coupling among the con-

stituent quarks and gluons is weak and perturbative (pQCD) calculations are possible, taking advantage of factorization theorems and evolution equations similar to quantum electrodynamics (QED). At the same time, QCD offers a clear path to unravel the non-perturbative structure of hadrons using lattice QCD,

a powerful *ab initio* numerical method that provides the best insight when the coupling among the constituents is strong.

The most fascinating property of QCD is confinement, which must arise from the dynamics of the partons inside hadrons. A small window into this dynamical behavior is offered by observables sensitive to quark-gluon correlations (providing confining forces) inside the spin- $\frac{1}{2}$ nucleon. An operator product expansion (OPE) provides well-defined quantities which codify not only the well known parton distributions in the nucleon, but also quark-gluon correlations lacking a naive partonic interpretation. Taking advantage of the spin- $\frac{1}{2}$ nucleon, these quantities can be measured in polarized inclusive deep inelastic electron scattering experiments and calculated as well, using lattice QCD (for review see [1]).

The principal focus of this Letter is the measurement of the dynamical twist-3 matrix element, \tilde{d}_2 , which is interpreted as an average transverse color Lorentz force [2] a quark feels due to the remnant at the space-time point just as it is struck by the virtual photon. Most importantly, a transversely polarized nucleon target probed with polarized electrons yields a unique experimental situation, where this color Lorentz force can be directly measured and used to test *ab initio* lattice QCD calculations.

This semi-classical interpretation of \tilde{d}_2 as an average transverse color Lorentz force is valid in the infinite momentum frame (IMF) of the proton, which is moving with velocity $\vec{v} = -c\hat{z}$. Using light-cone variables, the \hat{y} -component of the Lorentz force acting on a color charge g moving in the IMF is

$$g \left[\vec{E} + \vec{v} \times \vec{B} \right]^y = g \left[E_y + B_x \right] = g G^{+y} \quad (1)$$

where G^{+y} is a component of the gluon field strength tensor. Appearing in the definition of the local matrix element, G^{+y} connects \tilde{d}_2 to the semi-classical transverse force interpretation

$$\begin{aligned} F^y(0) &\equiv -\frac{\sqrt{2}}{2P^+} \langle P, S | \bar{q}(0) G^{+y}(0) \gamma^+ q(0) | P, S \rangle \\ &= -\sqrt{2} M P^+ S^x \tilde{d}_2 = -M^2 \tilde{d}_2, \end{aligned} \quad (2)$$

where the last equality is only valid in the proton's rest frame.

How do we access \tilde{d}_2 ? The nucleon spin structure functions, g_1 and g_2 , parameterize the asymmetric part of the hadronic tensor in inclusive electromagnetic scattering, which through the optical theorem, is related to the forward virtual Compton scattering amplitude, $T_{\mu\nu}$. The reduced matrix elements of the quark operators appearing in the OPE analysis of $T_{\mu\nu}$ are related to Cornwall-Norton (CN) moments [3] of the spin structure functions. At next-to-leading twist, the CN moments give

$$\int_0^1 x^{n-1} g_1(x, Q^2) dx = a_n + \mathcal{O}\left(\frac{M^2}{Q^2}\right), \quad n = 1, 3, \dots \quad (3)$$

and

$$\int_0^1 x^{n-1} g_2(x, Q^2) dx = \frac{n-1}{n} (d_n - a_n) + \mathcal{O}\left(\frac{M^2}{Q^2}\right), \quad (4)$$

$$n = 3, 5, \dots$$

where $a_n = \tilde{a}_{n-1}/2$ and $d_n = \tilde{d}_{n-1}/2$ are the twist-2 and twist-3 reduced matrix elements, respectively, which for increasing values of n have increasing dimension and spin¹. M is the nucleon mass and $Q^2 = -q^2$, where q^μ is the four-momentum transfer.

Neglecting target mass corrections (TMCs), *i.e.* $M^2/Q^2 \rightarrow 0$, the twist-3 matrix element can be extracted from the $n = 3$ CN moments

$$\tilde{d}_2 = \int_0^1 x^2 (3g_T(x) - g_1(x)) dx \quad (5)$$

where $g_T = g_1 + g_2$. The equation above shows how experimental access to \tilde{d}_2 is achieved through measurements of the spin structure functions g_1 and g_2 .

The famous Wandzura-Wilczek (WW) relation [4], $g_2^{WW}(x) = -g_1(x) + \int_x^1 g_1(y) dy/y$, allows us to write

$$g_T(x) = \int_x^1 \frac{dy}{y} g_1(y) + \bar{g}_2(x), \quad (6)$$

such that \bar{g}_2 contains the higher twist contribution to the g_2 spin structure function. In the limit of vanishing quark mass (5) can be evaluated using (3) and (4). In this limit, \bar{g}_2 contains only dynamical higher-twist contributions. At finite quark mass the WW relation still holds [5], however, g_T picks-up terms from the (twist-2) transversity parton distribution. These transversity contributions are the subject of recent theoretical investigations [6, 7].

Nachtmann moments should be used at low Q^2 instead of CN moments as is emphasized in [8]. Definitions of the Nachtmann moments, M_1^n and M_2^n , are found in [8–10] where they appear as more complicated versions of equations (3) and (4) which mix g_1 and g_2 . They are related to the reduced matrix elements through

$$M_1^{(n)}(Q^2) = a_n = \frac{\tilde{a}_{n-1}}{2}, \quad \text{for } n = 1, 3, \dots \quad (7)$$

$$M_2^{(n)}(Q^2) = d_n = \frac{\tilde{d}_{n-1}}{2}, \quad \text{for } n = 3, 5, \dots \quad (8)$$

¹ The twist of an operator is equal to its dimension minus its spin, and in QCD is a measure of the degree of interactions between the constituents of hadrons, with higher twist index representing increased correlations, e.g. the lowest twist, twist-2, corresponds to asymptotically free quarks; twist-3 is a quark-gluon-quark (qqq) correlation; twist-4 is some permutation of $qqgg$ correlations, etc. See [1] for a review.

where we use the convention of Dong². Nachtmann moments, by their construction, project out matrix elements of definite twist and spin, therefore, they do not contain any $\mathcal{O}(\frac{M^2}{Q^2})$ terms. When the target mass is neglected these equations reduce to $M_1^1 = \int g_1 dx$ and $2M_2^3 = \int x^2(2g_1 + 3g_2)dx$.

Because both twist-2 and twist-3 operators contribute at the same order in transverse polarized scattering, a measurement of g_2 provides *direct* access to higher twist effects[15] and thus the force we are seeking in this measurement. This puts polarized DIS in an entirely unique situation to test lattice QCD [16] and models of higher twist effects.

The Spin Asymmetries of the Nucleon Experiment (TJNAF E07-003) was conducted at Thomas Jefferson National Accelerator Facility in Hall-C during the winter of 2008-2009 using a longitudinally polarized electron beam and a polarized proton target. Inclusive inelastic scattering data in both the deep inelastic scattering and nucleon resonance regions were taken with two beam energies, $E = 4.7$ and 5.9 GeV, and with two target polarization directions: longitudinal, where the polarization direction was along the direction of the electron beam, and transverse, where the target polarization pointed in a direction perpendicular to the electron beam. The polarization angle with respect to the electron beam was 80° for the transverse configuration in order to match the acceptance and kinematics of scattered electrons in the longitudinal target configuration. Scattered electrons were detected in a new detector stack called the big electron telescope array (BETA) and also independently in Hall-C's high momentum spectrometer (HMS). Here, we give a brief discussion of the experimental apparatus and techniques, which are discussed in more details in an instrumentation paper [17].

The beam polarization was measured periodically using a Møller polarimeter and production runs had beam polarizations from 60% up to 90%. The beam helicity was flipped from parallel to anti-parallel at 30 Hz and the helicity state, determined at the accelerator's injector, was recorded for each event.

A polarized ammonia target acted as an effective polarized proton target and achieved an average polarization of 68% by dynamic nuclear polarization in a 5 T field. NMR measurements, calibrated against the calculable thermal equilibrium polarization, provided a continuous monitor of the target polarization. To mitigate local heating and depolarizing effects, the beam current

was limited to 100 nA and a raster system moved the beam in a 1 cm radius spiral pattern. By adjusting the microwave pumping frequency, the proton polarization direction was reversed. These two directions, positive and negative target polarizations, were used to estimate associated systematic uncertainties, since taking equal amounts of data with alternating positive and negative target polarization largely cancels any correlated behavior in the sum.

BETA consisted of four detectors: a forward tracker placed close to the target, a threshold gas Cherenkov counter, a Lucite hodoscope, and a large electromagnetic calorimeter called BigCal. BETA was placed at a fixed central scattering angle of 40° and covered a solid angle of roughly 200 msr. Electrons were identified by the Cherenkov counter, which had an average signal of roughly 18 photoelectrons[18]. The energy was determined by the BigCal calorimeter, which consisted of 1744 lead glass blocks placed 3.35 m from the target. BigCal was calibrated using a set of $\pi^0 \rightarrow \gamma\gamma$ events. The Lucite hodoscope provided additional timing and position event selection cuts and the forward tracker was not used in the analysis of production runs.

The 5 T polarized-target magnetic field caused large deflections for charged particle tracks. In order to reconstruct tracks at the primary scattering vertex, corrections to the momentum vector reconstructed at BigCal were calculated from a set of neural networks that were trained with simulated data sets for each configuration.

The invariant mass of the unmeasured final state is $W^2 = M^2 + 2M\nu - Q^2$, where M is the proton mass, $\nu = E - E'$ is the virtual photon energy, and $Q^2 = -q^2 = 2EE'(1 - \cos\theta)$. The scattered electron energy (E') and angle (θ) are used to calculate the Bjorken variable $x = Q^2/2M\nu$. BETA's large solid angle and open configuration allowed a broad kinematic range in x and Q^2 to be covered in a single setting.

The measured double spin asymmetries for longitudinal ($\alpha = 180^\circ$) and transverse ($\alpha = 80^\circ$) target configurations were formed using the yields for beam helicities pointing along (+) and opposite (−) the direction of the electron beam,

$$A_m(\alpha) \equiv \frac{1}{f(W, Q^2)P_B P_T} \left[\frac{N_+(\alpha) - N_-(\alpha)}{N_+(\alpha) + N_-(\alpha)} \right]. \quad (9)$$

The normalized yields are $N_\pm = n_\pm/(Q_\pm L_\pm)$, where n_\pm is the raw number of counts for each run (~ 1 hour of beam on target), Q_\pm is the accumulated charge for the given beam helicity over the counting period, and L_\pm is the live time for each helicity, $f(W, Q^2)$ is the target dilution factor, and the beam and target polarizations are P_B and P_T respectively. The target dilution factor, taking into account scattering from unpolarized nucleons in the target and depending on the scattered electron kinematics, is discussed in detail in [17].

² Some authors define the matrix elements excluding a factor of $1/2$ [9, 11–13], and/or use even n for the moments [5, 14]. In this work we use the convention of [8, 10] which absorbs the $1/2$ factor into the matrix element and use odd n for the moments, whereas, the matrix elements excluding the $1/2$ and even n are \tilde{a}_{n-1} and \tilde{a}_{n-1} .

The dominant source of background for this experiment came from the decay of π^0 's into two photons which, subsequently, produce electron-positron pairs which are then identified as DIS electrons. A pair produced outside of the target no longer experiences a strong magnetic field deflection, and therefore the pair travels in nearly the same direction. These events produced twice the amount of Čerenkov light and are effectively removed with a cut in maximum signal amplitude[18]. However, pairs produced inside the target are sufficiently and oppositely deflected, causing BETA to observe only one particle of the pair. These events cannot be removed through selection cuts and are treated through a background correction.

The background correction was determined by fitting existing inclusive π^0 production data and running a simulation to determine their contribution relative to the measured inclusive electron scattering yields. The correction only becomes significant at scattered energies below 1.2 GeV, where the positron-electron ratio begins to rise. The background correction consisted of a dilution (f_{BG}) and contamination (C_{BG}) term defined as

$$A_b(\alpha) = A_m(\alpha)/f_{BG} - C_{BG}. \quad (10)$$

The contamination term was small and only increases to 1% at the lowest x bin. The background dilution also increases at low x and becomes significant ($> 10\%$ of the measured asymmetry) only for $x < 0.35$.

After correcting for the pair symmetric background, the radiative corrections were applied following the standard formalism laid out by Mo and Tsai [19] and the polarization dependent treatment of Akushevich, et al. [20]. The elastic radiative tail was calculated from models of the proton form factor [21]. The pair-symmetric background-corrected asymmetry was then corrected with elastic dilution and contamination terms

$$A_{el}(\alpha) = A_b(\alpha)/f_{el} - C_{el}, \quad (11)$$

where f_{el} is the ratio of inelastic scattering to the sum of elastic and inelastic scattering, and C_{el} is the polarized elastic scattering cross section difference over the total inelastic cross section. The elastic dilution term remained less than 10% of the measured asymmetry in the range $x = 0.3$ to 0.8 for both target configurations. In the same range of x , the longitudinal configuration's elastic contamination remained less than 10% in absolute value, whereas, the transverse configuration's elastic contamination remained less than a few percent in absolute units.

The last correction required calculating the polarization dependent inelastic radiative tail of the Born-level polarization-dependent cross sections, which form the measured asymmetry. However, numerical studies [19, 22] with various models indicate the size of this radiative tail is small for most kinematics, reaching a few

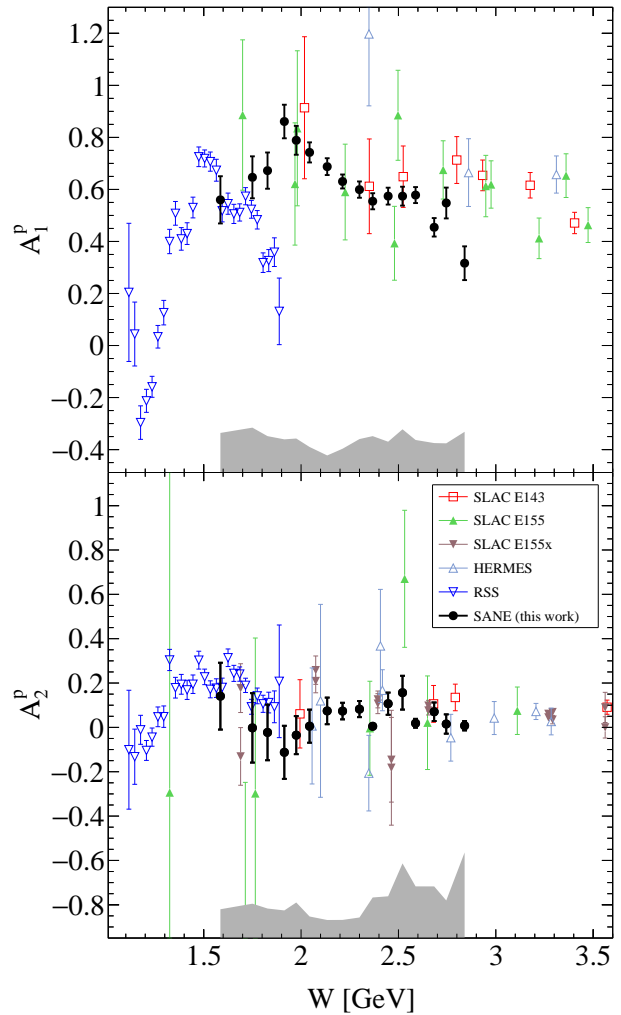


FIG. 1. The SANE results (circle) and existing data from SLAC's E143 (square)[23], E155 (filled up triangle) [24], E155x (filled down triangle)[25], HERMES (up triangle) [26], and RSS (down triangle) [27] experiments for the virtual Compton scattering asymmetries A_1^p (top) and A_2^p (bottom). The lower band shows systematic uncertainty. Note the A_1 data shown are from experiments which measured both $A_{||}$ and A_{\perp} .

percent only at the lowest and highest E' bins. More importantly, the contribution of this radiative tail to the inelastic asymmetry remains within the systematic uncertainties associated with the model and numerical precision of our calculations. Therefore, this correction was treated as a systematic uncertainty. This situation can only improve with future precision measurements of the polarization-dependent cross sections by scanning beam energies at a fixed angle [19].

The virtual Compton scattering asymmetries can be

written in terms of the measured asymmetries

$$A_1 = \frac{1}{D'} \left[\frac{E - E' \cos \theta}{E + E'} A_{180} + \frac{E' \sin \theta}{(E + E') \cos \phi} \frac{A_{180} \cos \alpha + A_\alpha}{\sin \alpha} \right] \quad (12)$$

and

$$A_2 = \frac{\sqrt{Q^2}}{2ED'} \left[A_{180} - \frac{E - E' \cos \theta}{E' \sin \theta \cos \phi} \frac{A_{180} \cos \alpha + A_\alpha}{\sin \alpha} \right] \quad (13)$$

with $\alpha = 80^\circ$ and where A_{180} and A_{80} are the corrected asymmetries, $D' = (1 - \epsilon)/(1 + \epsilon R)$, $\epsilon = (1 + 2(1 + \nu^2/Q^2) \tan^2(\theta/2))^{-1}$ is the degree of polarization of the longitudinal photon, and $R = \sigma_L/\sigma_T$ is the ratio of longitudinal to transverse unpolarized cross sections. The combined results for A_1 and A_2 versus W are shown in Fig. 1. These results significantly improve the world data on A_2^p . The spin structure functions can be obtained from the measured asymmetries by using equations (12) and (13) along with

$$g_1 = \frac{F_1}{1 + \gamma^2} (A_1 + \gamma A_2) \quad (14)$$

$$g_2 = \frac{F_1}{1 + \gamma^2} (A_2/\gamma - A_1), \quad (15)$$

where $\gamma^2 = Q^2/\nu^2$ and F_1 is the unpolarized structure function.

Table I lists the measured moments and corresponding integrated x ranges. The systematic uncertainties at the lower part of this range are dominated by the pair-symmetric background, which rapidly decreases towards higher x , where the target polarization, target dilution, and beam polarization uncertainties are most significant. Estimates for the low and high x contributions and their uncertainties were obtained from parton distribution fits to data [28–30] and fits to data in the resonance region [31]. In order to evaluate \tilde{d}_2 at a constant Q^2 , evolution equations for g_2 [32] were used to estimate a correction for each x point to provide g_2 at the same Q^2 , these corrections were found to be less than 1% for nearly all x points. It is important to note that the moments include the point at $x = 1$, which corresponds to elastic scattering on the nucleon. The elastic contributions to the moments are computed according to [33] using empirical fits to the electric and magnetic form factors [21]. At large Q^2 , the elastic contribution becomes negligible.

The results for the Nachtmann moment $2M_2^{(3)}(Q^2) = \tilde{d}_2(Q^2)$ are shown in Fig. 2 along with a comparison to the two previous measurements, lattice QCD results, and model calculations. The first measurement was extracted from the combined results of the SLAC E143, E155, and E155x experiments [25]. The SLAC and lattice results are consistent with our result at $Q^2 = 4.3 \text{ GeV}^2$. The

measurement from the Resonance Spin Structure (*RSS*) experiment (TJNAF E01-006) [27], extracted at $Q^2 = 1.28 \text{ GeV}^2$, has a value $\tilde{d}_2^p = 0.0104 \pm 0.0016$, of which, $\sim 1/3$ comes from the inelastic contribution.

At both $Q^2 = 2.8 \text{ GeV}^2$ and $Q^2 = 4.3 \text{ GeV}^2$ our proton \tilde{d}_2^p results are negative, although at $Q^2 = 4.3 \text{ GeV}^2$ it is consistent with zero. Interestingly, when considered together with the world data, these results suggest a non-trivial scale dependence of \tilde{d}_2 — positive at $Q^2 \sim 1 \text{ GeV}^2$ as reported by *RSS*, becoming negative around $Q^2 \sim 3 \text{ GeV}^2$ as indicated by this work, finally, increasing slowly toward the positive SLAC measurement at $Q^2 = 5 \text{ GeV}^2$ — in contrast to the monotonic behavior expected from twist-3 pQCD evolution [32, 34]. Furthermore, with the exception of the QCD sum rules, all model calculations and lattice QCD give positive values for the proton \tilde{d}_2^p . Intriguingly, our results complement a recent neutron \tilde{d}_2^n measurement [35, 36], which shows a sizable negative value at $Q^2 \sim 3 \text{ GeV}^2$, equal to that of the proton, as shown in Fig. 2. We note that while both experiments were performed at Jefferson Lab they used completely independent apparatus in two different Halls. Our proton results in combination with the world neutron results point to a flavor independent average color Lorentz force that has a puzzling scale dependence in contrast with recent expectations [2].

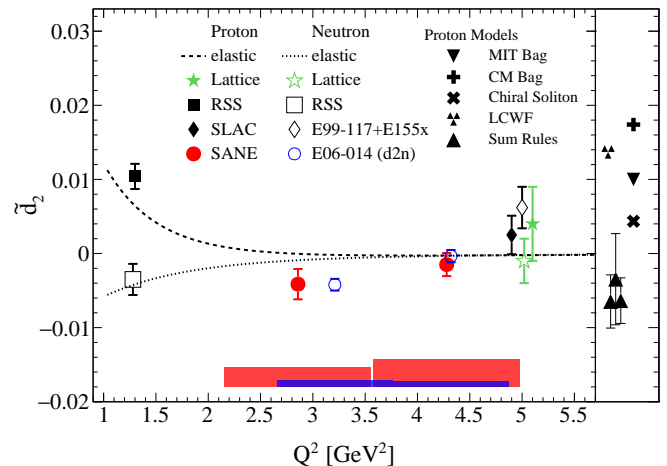


FIG. 2. The results for \tilde{d}_2 of the proton from this work (SANE) and recent neutron results [35] with their systematic uncertainties (displayed in the lower bands). Also shown are the lattice QCD results [16], previous proton (neutron) measurements with filled (open) symbols from SLAC [25], E99-117 and E155x [37], and *RSS* [27, 38] experiments. The dashed (dotted) lines show the elastic contribution for the proton (neutron). The panel on the right shows proton model calculations from QCD sum rules [39, 40], the bag model [41], the Center-of-Mass (CM) bag model [42], the chiral soliton model [43], and light-cone wave functions (LCWF) [44]. The models are calculated at $Q^2 = 5 \text{ GeV}^2$, except the sum rules and LCWF, which were evaluated at $Q^2 = 1 \text{ GeV}^2$.

In summary, the proton's spin structure functions g_1

TABLE I. Results for $\tilde{d}_2 = 2M_2^3$ in units of $\times 10^{-3}$ with their statistical and systematic uncertainties. The low x , high x , and elastic systematic uncertainties were obtained from models. See text for details.

$x_{\text{low}} - x_{\text{high}}$	$\langle Q^2 \rangle = 2.8 \text{ GeV}^2$		$\langle Q^2 \rangle = 4.3 \text{ GeV}^2$	
	0.26 – 0.57		0.44 – 0.74	
	(stat.)	(sys.)	(stat.)	(sys.)
measured	$-4.77 \pm 2.05 \pm 1.81$		$-3.22 \pm 1.56 \pm 3.57$	
low x	1.86	± 0.13	2.47	± 0.54
high x	-1.19	± 1.81	-0.49	± 0.72
elastic	-0.04	± 0.01	-0.25	± 0.02
total	$-4.14 \pm 2.05 \pm 2.56$		$-1.49 \pm 1.56 \pm 3.68$	

and g_2 have been measured at kinematics allowing for an extraction of \tilde{d}_2 at two different values of Q^2 . The present results in combination with the world data suggest an unexpected scale dependence of the average color Lorentz force and a flavor independence. Furthermore, precision measurements at 12 GeV Jefferson Lab with transversely polarized proton and neutron targets are justified to confirm this puzzling behavior [45–47]. Moreover modern lattice QCD calculations of \tilde{d}_2 , without the quenched approximation, which include disconnected diagrams [16], and are performed at the physical pion mass without chiral extrapolation, are sorely needed for a complete understanding of our observation.

We would like to thank Vladimir Braun and Matthias Burkardt for discussions and feedback during the revision process. We would like to express our gratitude to the staff and technicians of Jefferson Lab for their support during the running of SANE. We especially thank the Hall C and Target Group personnel, who saw a technically challenging experiment through significant hardship to a successful end. This work was supported in part by the U.S. Department of Energy, Office of Science, Office of Nuclear Physics, under contract no. DE-AC02-06CH11357, DE-FG02-94ER4084, DE-FG02-96ER40950, and DE-AC05-06OR23177.

* Deceased.

- [1] R. L. Jaffe, in *The spin structure of the nucleon. Proceedings, International School of Nucleon Structure, 1st Course, Erice, Italy, August 3-10, 1995* (1996) pp. 42–129, arXiv:hep-ph/9602236 [hep-ph].
- [2] M. Burkardt, Phys. Rev. **D88**, 114502 (2013), arXiv:0810.3589 [hep-ph].
- [3] J. M. Cornwall and R. E. Norton, Phys. Rev. **177**, 2584 (1969).
- [4] S. Wandzura and F. Wilczek, Phys. Lett. **72B**, 195 (1977).
- [5] J. Blumlein and A. Tkabladze, Nucl. Phys. **B553**, 427 (1999), arXiv:hep-ph/9812478 [hep-ph].

- [6] A. Accardi, A. Bacchetta, W. Melnitchouk, and M. Schlegel, JHEP **11**, 093 (2009), arXiv:0907.2942 [hep-ph].
- [7] A. Accardi and A. Bacchetta, Phys. Lett. **B773**, 632 (2017), arXiv:1706.02000 [hep-ph].
- [8] Y. B. Dong, Phys. Rev. **C78**, 028201 (2008), arXiv:0811.1002 [hep-ph].
- [9] S. Matsuda and T. Uematsu, Nucl. Phys. **B168**, 181 (1980).
- [10] A. Piccione and G. Ridolfi, Nucl. Phys. **B513**, 301 (1998), arXiv:hep-ph/9707478 [hep-ph].
- [11] J. Kodaira, S. Matsuda, T. Muta, K. Sasaki, and T. Uematsu, Phys. Rev. **D20**, 627 (1979).
- [12] J. Kodaira, Nucl. Phys. **B165**, 129 (1980).
- [13] J. Kodaira, S. Matsuda, K. Sasaki, and T. Uematsu, Nucl. Phys. **B159**, 99 (1979).
- [14] R. L. Jaffe and X.-D. Ji, Phys. Rev. **D43**, 724 (1991).
- [15] R. L. Jaffe, Comments Nucl. Part. Phys. **19**, 239 (1990).
- [16] M. Gockeler, R. Horsley, D. Pleiter, P. E. L. Rakow, A. Schafer, G. Schierholz, H. Stuben, and J. M. Zanotti, Phys. Rev. **D72**, 054507 (2005), arXiv:hep-lat/0506017 [hep-lat].
- [17] J. D. Maxwell *et al.*, Nucl. Instrum. Meth. **A885**, 145 (2018), arXiv:1711.09089 [physics.ins-det].
- [18] W. R. Armstrong, S. Choi, E. Kaczanowicz, A. Lukhanin, Z.-E. Meziani, and B. Sawatzky, Nucl. Instrum. Meth. **A804**, 118 (2015), arXiv:1503.03138 [physics.ins-det].
- [19] L. W. Mo and Y.-S. Tsai, Rev. Mod. Phys. **41**, 205 (1969).
- [20] I. V. Akushevich and N. M. Shumeiko, J. Phys. **G20**, 513 (1994).
- [21] J. Arrington, W. Melnitchouk, and J. A. Tjon, Phys. Rev. **C76**, 035205 (2007), arXiv:0707.1861 [nucl-ex].
- [22] I. Akushevich, A. Ilyichev, N. Shumeiko, A. Soroko, and A. Tolmachev, Comput. Phys. Commun. **104**, 201 (1997).
- [23] K. Abe *et al.* (E143), Phys. Rev. Lett. **78**, 815 (1997), arXiv:hep-ex/9701004 [hep-ex].
- [24] P. L. Anthony *et al.* (E155), Phys. Lett. **B458**, 529 (1999), arXiv:hep-ex/9901006 [hep-ex].
- [25] P. L. Anthony *et al.* (E155), Phys. Lett. **B553**, 18 (2003), arXiv:hep-ex/0204028 [hep-ex].
- [26] A. Airapetian *et al.* (HERMES), Eur. Phys. J. **C72**, 1921 (2012), arXiv:1112.5584 [hep-ex].
- [27] K. Slifer *et al.* (Resonance Spin Structure), Phys. Rev. Lett. **105**, 101601 (2010), arXiv:0812.0031 [nucl-ex].
- [28] J. Blumlein and H. Bottcher, Nucl. Phys. **B636**, 225 (2002), arXiv:hep-ph/0203155 [hep-ph].
- [29] C. Bourrely and J. Soffer, Nucl. Phys. **A941**, 307 (2015), arXiv:1502.02517 [hep-ph].
- [30] N. Sato, W. Melnitchouk, S. E. Kuhn, J. J. Ethier, and A. Accardi (Jefferson Lab Angular Momentum), Phys. Rev. **D93**, 074005 (2016), arXiv:1601.07782 [hep-ph].
- [31] D. Drechsel, S. S. Kamalov, and L. Tiator, Eur. Phys. J. **A34**, 69 (2007), arXiv:0710.0306 [nucl-th].
- [32] V. M. Braun, G. P. Korchemsky, and A. N. Manashov, Nucl. Phys. **B603**, 69 (2001), arXiv:hep-ph/0102313 [hep-ph].
- [33] W. Melnitchouk, R. Ent, and C. Keppel, Phys. Rept. **406**, 127 (2005), arXiv:hep-ph/0501217 [hep-ph].
- [34] E. V. Shuryak and A. I. Vainshtein, Nucl. Phys. **B201**, 141 (1982).
- [35] D. Flay *et al.* (Jefferson Lab Hall A), Phys. Rev. **D94**, 052003 (2016), arXiv:1603.03612 [nucl-ex].
- [36] M. Posik *et al.* (Jefferson Lab Hall A), Phys. Rev. Lett.

- 113**, 022002 (2014), arXiv:1404.4003 [nucl-ex].
- [37] X. Zheng *et al.* (Jefferson Lab Hall A), Phys. Rev. **C70**, 065207 (2004), arXiv:nucl-ex/0405006 [nucl-ex].
 - [38] F. R. Wesselmann *et al.* (RSS), Phys. Rev. Lett. **98**, 132003 (2007), arXiv:nucl-ex/0608003 [nucl-ex].
 - [39] I. I. Balitsky, V. M. Braun, and A. V. Kolesnichenko, Phys. Lett. **B242**, 245 (1990), [Erratum: Phys. Lett. B318,648(1993)], arXiv:hep-ph/9310316 [hep-ph].
 - [40] E. Stein, P. Gornicki, L. Mankiewicz, A. Schafer, and W. Greiner, Phys. Lett. **B343**, 369 (1995), arXiv:hep-ph/9409212 [hep-ph].
 - [41] A. I. Signal, Nucl. Phys. **B497**, 415 (1997), arXiv:hep-ph/9610480 [hep-ph].
 - [42] X. Song, Phys. Rev. **D54**, 1955 (1996), arXiv:hep-ph/9604264 [hep-ph].
 - [43] H. Weigel, L. P. Gamberg, and H. Reinhardt, Phys. Rev. **D55**, 6910 (1997), arXiv:hep-ph/9609226 [hep-ph].
 - [44] V. M. Braun, T. Lautenschlager, A. N. Manashov, and B. Pirnay, Phys. Rev. **D83**, 094023 (2011), arXiv:1103.1269 [hep-ph].
 - [45] T. Averett, W. Korsch, Z.-E. Meziani, and B. Sawatzky, “E12-06-121,” (2006), approved JLab experiment in Hall C.
 - [46] H. Gao, X. Qian, J.-P. Chen, and Z.-E. Meziani, “E12-10-006,” (2009), approved JLab experiment using SoLID spectrometer.
 - [47] H. Gao, K. Allada, J.-P. Chen, and Z.-E. Meziani, “E12-11-108,” (2009), approved JLab experiment using SoLID spectrometer.